# On the Structure of Vanadium Oxide Supported on Aluminas: UV and Visible Raman Spectroscopy, UV−Visible Diffuse Reflectance Spectroscopy, and Temperature-Programmed Reduction Studies

**Zili Wu,[†] Hack-Sung Kim,[†] Peter C. Stair,*[,†] Sreekala Rugmini,[‡] and S. David Jackson[‡]**

*Department of Chemistry, Center for Catalysis and Surface Science and Institute of Environmental Catalysis, Northwestern University, Evanston, Illinois 60208, and Department of Chemistry, Joseph Black Building, The University, Glasgow G12 8QQ, Scotland, U.K.*

*Received: September 3, 2004; In Final Form: December 7, 2004*

Vanadia species on aluminas ($\delta$- and $\gamma$-$Al_2O_3$) with surface $VO_x$ density in the range 0.01−14.2 V/nm$^2$ have been characterized by UV and visible Raman spectroscopy, UV−visible diffuse reflectance spectroscopy (UV−Vis DRS), and temperature-programmed reduction in hydrogen. It is shown that the alumina phase has little influence on the structure and reducibility of surface $VO_x$ species under either dehydrated or hydrated conditions. Three similar types of dispersed $VO_x$ species, i.e., monovanadates, polyvanadates, and $V_2O_5$, are identified on both aluminas under dehydrated conditions. Upon hydration, polymerized $VO_x$ species dominate on the surfaces of the two aluminas. The broad Raman band at around 910 cm$^{-1}$, observed on dehydrated V/$\delta$-, $\gamma$-$Al_2O_3$ at all V loadings (0.01−14.2 V/nm$^2$), is assigned to the interface mode (V−O−Al) instead of the conventionally assigned V−O−V bond. The direct observation of the interface bond is of significance for the understanding of redox catalysis because this bond has been considered to be the key site in oxidation reactions catalyzed by supported vanadia. Two types of frequency shifts of the V═O stretching band (1013−1035 cm$^{-1}$) have been observed in the Raman spectra of V/$Al_2O_3$: a shift as a function of surface $VO_x$ density and a shift as a function of excitation wavelength. The shift of the V═O band to higher wavenumbers with increasing surface $VO_x$ density is due to the change of $VO_x$ structure. The V═O stretching band in dispersed vanadia always appears at lower wavenumber in UV Raman spectra than in visible Raman spectra for the same V/$Al_2O_3$ sample. This shift is explained by selective resonance enhancement according to the UV−Vis DRS results. It implies that UV Raman has higher sensitivity to isolated and less polymerized $VO_x$ species while visible Raman is more sensitive to highly polymerized $VO_x$ species and crystalline $V_2O_5$. These results show that a multiwavelength excitation approach provides a more complete structural characterization of supported $VO_x$ catalysts.

## 1. Introduction

Supported vanadia catalysts have attracted significant interest in recent decades due to their good catalytic performance in many redox reactions[1−6] such as dehydrogenation and oxidative dehydrogenation of alkanes to olefins, oxidation of methanol to formaldehyde, ammoxidation of aromatic hydrocarbons, and selective reduction of $NO_x$. A better understanding of the catalytic properties of supported vanadium oxides requires determination of the structure−reactivity relationships of the supported $VO_x$ catalysts. Raman spectroscopy has been successfully and frequently employed by many research groups for characterization of the molecular structure of supported vanadium oxides.[2,4−18] For vanadia supported on most oxide supports, e.g., $SiO_2$, $Al_2O_3$, $TiO_2$, $ZrO_2$, MgO, etc., three types of surface vanadia species have been identified by Raman spectroscopy: isolated vanadia, polymerized vanadia, and crystalline $V_2O_5$. The presence of these species is a function of $VO_x$ loading, the nature of the support, and the ambient environment.[2,4−11,15] Three kinds of bonds between vanadium and oxygen are present in these $VO_x$ species: V═O, V−O−V, and V−O−S (S, support). It is generally accepted that the bridging V−O−S bond is critical for redox reactions catalyzed by supported $VO_x$.[4−6,13,18] The discrimination of different surface $VO_x$ species has generally been based on their characteristic Raman features. Isolated and polymerized $VO_x$ species have been characterized by sharp V═O stretching bands in the range 900−1050 cm$^{-1}$; broad Raman features in the range 500−950 cm$^{-1}$ have been attributed to V−O−V stretching in polymerized $VO_x$, and the presence of $V_2O_5$ is indicated by an intense V═O stretching band at 995 cm$^{-1}$. The catalytic properties of supported $VO_x$ catalysts have been shown to be sensitive to the distribution of these surface $VO_x$ species.[4−6,10,13,15]

It is notable that most Raman studies of supported $VO_x$ catalysts were carried out using a single excitation wavelength in the visible region (either 514 or 532 nm).[3−15] However, several recent investigations on supported transition-metal oxides,[16,17,19,20] including vanadium oxides[16,17] under ambient conditions, using both UV and visible wavelength Raman excitations suggest that more complete and sometimes new structural information of supported metal oxides can be achieved by using multiple excitation wavelengths. The reason lies in the strong electronic absorptions in the UV and visible wavelength regions exhibited by most transition-metal oxides which make it possible to measure resonance-enhanced Raman spectra. Under circumstances where supported $VO_x$ species are present in a distribution of cluster sizes or coordination

* Author to whom correspondence may be addressed. Email: pstair@northwestern.edu.
[†] Northwestern University.
[‡] The University.

10.1021/jp046011m CCC: $30.25 
Published on Web 02/02/2005

geometries, it is likely that these species also possess a corresponding distribution of electronic absorption wavelengths. Excitation of Raman spectra within the absorption region will produce resonance-enhanced spectra from the subset of $VO_x$ species with absorptions at the excitation wavelength. Through measurement of the Raman spectra at several wavelengths, more information can be obtained about the various $VO_x$ species in the distribution. Moreover, when UV excitation is employed, even Raman spectra from supported $VO_x$ at low loadings (<1wt %) on oxides having strong fluorescence are possible because of the avoidance of fluorescence and enhanced sensitivity.[21,22]

The present work is aimed at a further study of the structure of $VO_x$ supported on alumina using both UV (244 nm) and visible (488 nm) excited Raman spectroscopy and especially the structure of supported $VO_x$ at extremely low surface density (down to 0.01 V/nm$^2$). The V/$Al_2O_3$ samples were studied under both hydrated and dehydrated conditions. Interpretation of the Raman spectra was also aided by UV−visible diffuse reflectance spectroscopy (UV−Vis DRS) and temperature-programmed reduction (TPR) measurements. Two different aluminas, $\delta$- and $\gamma$-$Al_2O_3$, were selected as the supports in order to investigate the influence of different alumina phases (environments) on the structure of surface $VO_x$ species. It is our intention to use these supported $VO_x$ materials as catalysts for alkane dehydrogenation, and with this in mind, the suitability of various alumina phases was considered. Since the dehydrogenation reaction operates near the temperature for phase transition from $\gamma$-$Al_2O_3$ to $\delta$-$Al_2O_3$,[23,24] the $\delta$-alumina phase is expected to be more stable for dehydrogenation reactions. Therefore, we were motivated to compare V/$\delta$-$Al_2O_3$ to the more extensively studied V/$\gamma$-$Al_2O_3$ system.

## 2. Experimental Section

**2.1. Sample Preparation.** All supported $VO_x$ samples were prepared via incipient wetness impregnation of aluminas with aqueous $NH_4VO_3$ (99+%, Aldrich) solutions. Oxalic acid (99%, Aldrich) ($NH_4VO_3$/oxalic acid = 0.5 molar) was added into the solutions for high $VO_x$ loadings to ensure the dissolution of $NH_4VO_3$. Two types of aluminas were used: $\delta$-$Al_2O_3$ (Johnson Matthey, UK, $S_{BET}$ = 101 m$^2$/g) and $\gamma$-$Al_2O_3$ (Engelhard, $S_{BET}$ = 220 m$^2$/g). The surface area ($S_{BET}$) data were provided by the manufacturers. Because of differences in surface area of the aluminas, surface $VO_x$ density (V/nm$^2$) instead of surface $VO_x$ loading (wt %) is used to describe the supported $VO_x$ samples. A V/$Al_2O_3$ sample with surface $VO_x$ density of Y V/nm$^2$ will be denoted as YV in the following text. After impregnation, the samples were dried at room temperature by purging with air and then heated at 393 K overnight. Finally, the samples were calcined at higher temperature (823 K for V/$\delta$-$Al_2O_3$ and 773 K for V/$\gamma$-$Al_2O_3$) for 6 h in air.

**2.2. Raman Studies.** Both UV (244 nm) and visible (488 nm) Raman spectra of V/$Al_2O_3$ samples were collected using the UV Raman instrument built at Northwestern University[17,21,22] under dehydrated and hydrated conditions. The 244-nm line is from a Lexel 95 SHG (second harmonic generation) laser equipped with an intracavity nonlinear crystal, BBO ($\beta$-barium borate: BaB2O4), that frequency doubled visible radiation into the mid-ultraviolet region. The 488-nm line is obtained by removing the BBO crystal and replacing the UV output coupler by a visible one in the Lexel 95 SHG laser. Because the grating settings in the spectrometer are optimized for Raman scattering near the 244-nm region, the spectral range for visible Raman (~260 cm$^{-1}$) study on the same spectrometer is much narrower than that of UV Raman (~1500 cm$^{-1}$). Consequently, the spectra obtained using 488-nm excitation are displayed in the range 820−1070 cm$^{-1}$. This region contains the strongest and most informative Raman bands of supported $VO_x$ and provides the best comparison to UV Raman spectra.

Raman spectra of dehydrated samples were collected under a controlled atmosphere using a fluidized bed reactor designed in this lab.[25] The V/$Al_2O_3$ samples were heated in the fluidized bed reactor in flowing 5% $O_2$/$N_2$ (60 mL/min) at high temperatures (823 K for V/$\delta$-$Al_2O_3$ and 773 K for V/$\gamma$-$Al_2O_3$) for 2 h to remove adsorbed moisture. Raman spectra were then taken at room temperature in flowing He (>100 mL/min). Hydrated samples were obtained by exposing the calcined samples to ambient conditions for at least 2 days, and spectra were measured from powder samples loaded in a cap spinning at ~2000 rpm. The laser power at the sample position was ~2 mW for 244-nm irradiation and ~20 mW for 488-nm irradiation. Data collection times varied from 600 s to 6 h depending on the signal level. The Raman shift was calibrated by measuring several liquid standards including cyclohexane, acetonitrile, chloroform, ethyl acetate, toluene, and benzene. A mathematical procedure involving a quadratic fit of the observed to the actual wavenumbers of the standards was employed. The band positions in the Raman spectra were determined using the program PeakFit v4.11.

Interference from laser-induced changes of the V/$Al_2O_3$ samples under 488- and 244-nm irradiation was examined. Spectra were recorded under a controlled atmosphere and using a variety of conditions, including an experiment where the two lasers simultaneously irradiated the same area of the sample. There was never any indication of laser-induced changes to the sample.

**2.3. UV−Vis DRS Measurements.** DRS spectra in the range of 200−800 nm were taken on a Varian Cary 1E UV−vis spectrophotometer equipped with a diffuse-reflectance attachment, using MgO as a reference. The spectra of hydrated samples were collected under ambient conditions. For dehydrated samples, the V/$Al_2O_3$ sample was first calcined in an oven at 723 K for 2 h and then transferred into a desiccator and later into a glovebox. The sample was sealed into a small vial that is transparent in the range 200−800 nm, and the UV−vis DRS spectrum was measured at room temperature.

**2.4. TPR.** $H_2$ TPR of V/$\delta$- and $\gamma$-$Al_2O_3$ was carried out in a $H_2$/Ar (5%) flow of 40 mL/min from room temperature to 1023 K with a ramp of 8 K/min. Prior to this, the samples (ca. 100 mg) were treated for 1 h at 773 K in pure $O_2$, cooled to room temperature, and purged with Ar for at least 30 min. The $H_2$ consumption was determined by a TCD detector, with $H_2O$ being trapped in a dry ice-cooled trap.

## 3. Results

**3.1. Raman Spectra.** *3.1.1. V/$\delta$-$Al_2O_3$.* Visible Raman spectra of dehydrated V/$\delta$-$Al_2O_3$ samples are presented in Figure 1A, which also includes the spectra of $\delta$-$Al_2O_3$ and $V_2O_5$ for comparison. The spectra of V/$\delta$-$Al_2O_3$ with surface $VO_x$ density lower than 0.16 V/nm$^2$ are dominated by fluorescence from the $\delta$-$Al_2O_3$ support. At a surface $VO_x$ density of 0.16 V/nm$^2$, a weak Raman band is observed at 1023 cm$^{-1}$ and a broad Raman feature appears at ca. 915 cm$^{-1}$. The broad band at 915 cm$^{-1}$ is present for all samples and becomes weaker at higher surface $VO_x$ density. The band at 1023 cm$^{-1}$ shifts to higher wavenumbers and becomes very weak with increasing surface $VO_x$ density. An intense Raman band at 995 cm$^{-1}$ characteristic of crystalline $V_2O_5$ appears at a surface $VO_x$ density of 4.4 V/nm$^2$ and above (parts e−g of Figure 1A). At a surface $VO_x$ density

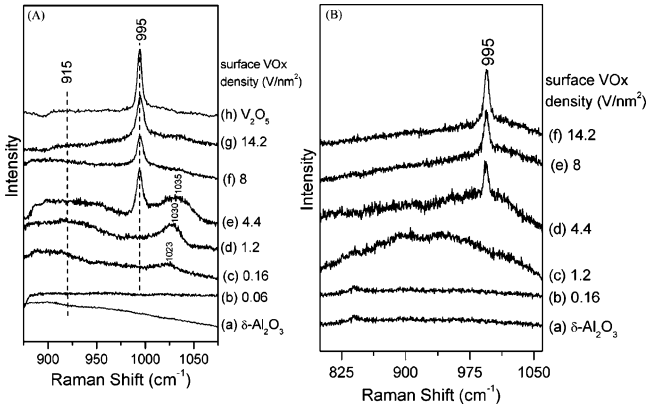


**Figure 1.** Visible ($\lambda_{excitation}$ = 488 nm) Raman spectra of dehydrated (A) and hydrated (B) V/$\delta$-$Al_2O_3$ as a function of surface $VO_x$ density (V/nm$^2$).

of 8 V/nm$^2$, which is approximately monolayer coverage for $VO_x$ on $Al_2O_3$,[6,8,12,26] the Raman band of $V_2O_5$ is very intense, and the other two bands at 1035 and 915 cm$^{-1}$ become very weak.

The Raman band at ca. 1023 cm$^{-1}$ can be assigned to the V═O stretching mode of surface $VO_x$ species. The broad band at ~915 cm$^{-1}$ has previously been ascribed to V—O—V stretching modes and used as a proof for the presence of polymerized $VO_x$ species.[4−15] Here we assign it to the interface mode, V—O—Al, in accordance with recent DFT calculations of the $VO_x$−$Al_2O_3$ system.[27] This assignment is confirmed by the UV Raman results described below.

Figure 1B shows the Raman spectra of hydrated V/$\delta$-$Al_2O_3$ which are quite different from those of the dehydrated samples. No Raman feature can be observed for the samples with surface $VO_x$ density below 1.2 V/nm$^2$. At 1.2 V/nm$^2$, a very broad Raman feature appears, centered at 930 cm$^{-1}$ and extending over the spectral range of 800−1050 cm$^{-1}$. At higher density, this feature becomes weaker and evolves into a shoulder on the lower wavenumber side of the $V_2O_5$ band at 994 cm$^{-1}$. With the exception of a change in the background slope, the Raman spectrum of $V_2O_5$ is essentially identical for hydrated and dehydrated samples. The broad Raman feature may be due to surface polyvanadates on $\delta$-$Al_2O_3$.[8,11,28,29] The absence of Raman bands above 1000 cm$^{-1}$ due to V═O vibration in Figure 1B is attributed to hydrolysis of the V═O bond by water adsorbed from the atmosphere.

Figure 2A shows the UV Raman spectra of dehydrated V/$\delta$-$Al_2O_3$ with surface $VO_x$ density varying from 0.01 to 14.2 V/nm$^2$. Two bands of medium intensity at 837 and 740 cm$^{-1}$ are observed for the $\delta$-$Al_2O_3$ support. The two bands decline in intensity with increasing surface $VO_x$ density and disappear at a surface $VO_x$ density of 0.16 V/ nm$^2$. This is attributed to strong absorption of the UV radiation by surface $VO_x$ species (see following UV−vis DRS results).

It is striking to note that some Raman features due to surface $VO_x$ species can be distinguished for V/$\delta$-$Al_2O_3$ samples at extremely low surface density even down to 0.01 V/nm$^2$, i.e., a weak Raman band at 1013 cm$^{-1}$ and a broad shoulder at around 912 cm$^{-1}$ (Figure 2Ab). These Raman features cannot be detected in the visible Raman spectra (see Figure 1) and have not been reported by previous Raman studies. The broad feature centered at 912 cm$^{-1}$ is present with medium intensity at all loadings, suggesting that this broad Raman feature cannot be exclusively assigned to V—O—V stretching. The 1013-cm$^{-1}$ band, assigned to the V═O stretching mode of surface $VO_x$ species, shifts gradually to a higher wavenumber as the surface $VO_x$ density increases. This band remains observable at ca. 1026 cm$^{-1}$ for a surface $VO_x$ density of 14.2 V/nm$^2$, a result which is clearly different from the visible Raman spectra (Figure 1) where the V═O band is above 1030 cm$^{-1}$ for surface $VO_x$ densities greater than 1.2 V/nm$^2$ and disappears above monolayer loading (8 V/nm$^2$). The differences in Raman shift and in intensity vs $VO_x$ density between visible- and UV-excited Raman spectra suggest the presence of different types of surface $VO_x$ species on the $Al_2O_3$ support. At medium surface $VO_x$ densities (0.16−4.4 V/nm$^2$), a weak broad feature appears near 625 cm$^{-1}$. This band is attributed to symmetric stretching of V—O—V chains,[3−15] indicating the formation of polymerized $VO_x$ species on the surface. When the surface $VO_x$ density is above 8 V/nm$^2$, the formation of crystalline $V_2O_5$ is evident from the characteristic band at 994 cm$^{-1}$ and additional bands in the range 400−600 cm$^{-1}$.

UV Raman spectra of hydrated V/$\delta$-$Al_2O_3$ are shown in Figure 2B. In a manner similar to the visible spectra (Figure 1B), Raman bands above 1000 cm$^{-1}$ due to terminal V═O vibrations disappear upon hydration for all V/$\delta$-$Al_2O_3$ samples. V/$\delta$-$Al_2O_3$ samples with low surface density show a broad feature at around 910 cm$^{-1}$. The band maximum shifts to higher wavenumbers with increased surface density, i.e., to 930 cm$^{-1}$ for 1.2 V, to 980 cm$^{-1}$ for 4.4 V, and up to 995 cm$^{-1}$ for 8- and 14.2-V samples. A broad band at ~550 cm$^{-1}$ is also observed at intermediate surface density (parts d−f of Figure 2B). These broad Raman features imply the presence of polyvanadate species on the surface of hydrated V/$\delta$-$Al_2O_3$.[3−6,8]

*3.1.2. V/$\gamma$-$Al_2O_3$.* Parts A and B of Figure 3 present the visible Raman spectra of dehydrated and hydrated V/$\gamma$-$Al_2O_3$ samples,

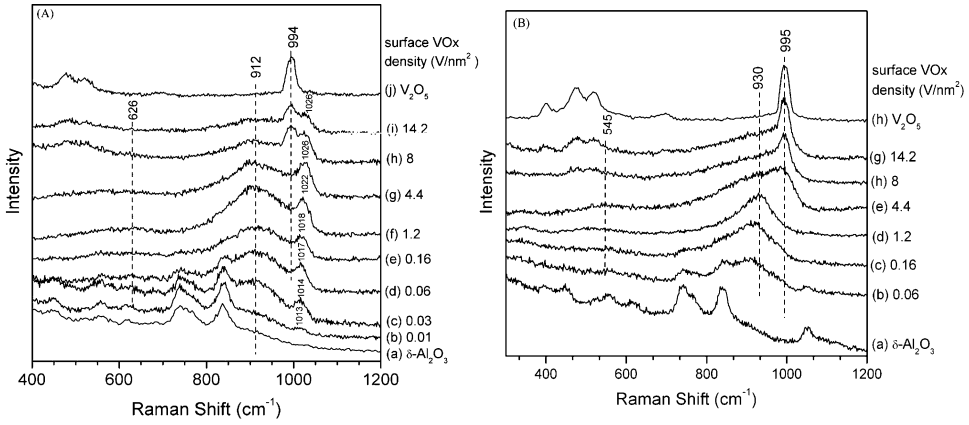


**Figure 2.** UV ($\lambda_{excitation}$ = 244 nm) Raman spectra of dehydrated (A) and hydrated (B) V/$\delta$-$Al_2O_3$ as a function of surface $VO_x$ density (V/nm$^2$).

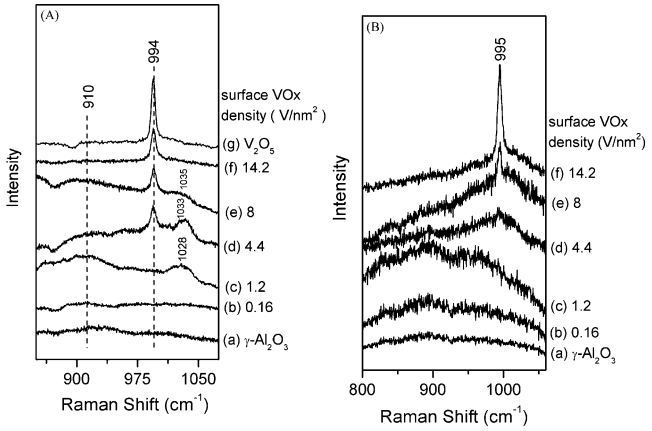


**Figure 3.** Visible ($\lambda_{excitation}$ = 488 nm) Raman spectra of dehydrated (A) and hydrated (B) V/$\gamma$-$Al_2O_3$ as a function of surface $VO_x$ density (V/nm$^2$).

respectively. Dehydrated samples (Figure 3A) with surface densities above 0.16 V/nm$^2$ show Raman bands due to $VO_x$ species: a weak broad band centered at 910 cm$^{-1}$ due to the V—O—Al mode, a V═O vibration at 1028 cm$^{-1}$ for 1.2 V and 1034 cm$^{-1}$ for 4.4- and 8.8-V samples, and an intense band at 994 cm$^{-1}$ characteristic of $V_2O_5$ for 4.4 V and above. For hydrated samples, a broad Raman feature centered at 900 cm$^{-1}$ covers the whole spectral range (800−1050 cm$^{-1}$) at surface $VO_x$ densities of 0.16 and 1.2 V/nm$^2$. It becomes a shoulder on the lower wavenumber side of the $V_2O_5$ band at 994 cm$^{-1}$ at higher $VO_x$ density.

UV Raman spectra of dehydrated and hydrated V/$\gamma$-$Al_2O_3$ are, respectively, shown in parts A and B of Figure 4. $\gamma$-$Al_2O_3$ gives rise to a broad Raman band at ∼855 cm$^{-1}$ in both hydrated and dehydrated states. It is obvious that the changes in UV Raman spectra as a function of surface $VO_x$ density on $\gamma$-$Al_2O_3$ (parts A and B of Figure 4) exhibit similar trends to those on $\delta$-$Al_2O_3$ (parts A and B of Figure 2). Briefly, for dehydrated V/$\gamma$-$Al_2O_3$ samples, the broad Raman feature at ∼910 cm$^{-1}$ is present on all samples; the V═O vibration mode of surface $VO_x$ species gives Raman bands in the range 1012−1027 cm$^{-1}$; a broad Raman feature due to V—O—V stretching at ∼630 cm$^{-1}$ appears at intermediate surface $VO_x$ density, and $V_2O_5$ forms on the surface at and above monolayer density (8 V/nm$^2$). For hydrated samples, broad bands in the range 910−995 cm$^{-1}$ are observed from low surface density to high surface density, which are due to hydrated, polymerized $VO_x$ species.[8,11] The polymerized $VO_x$ species are also characterized by the broad Raman feature at ∼545 cm$^{-1}$ (parts c−e of Figure 4B).

**3.2. UV−Vis DRS Spectra.** UV−Vis spectra of dehydrated and hydrated V/$\delta$-$Al_2O_3$ are shown in parts A and B of Figure 5, respectively. In both figures, the main electronic absorption band shifts to higher wavelengths and becomes broader with increasing surface $VO_x$ density. The broad band is due to the charge-transfer transition between oxygen ligands and vanadium metal centers.[30] The dehydrated samples with low surface $VO_x$ density (<1.2 V/nm$^2$) show absorption primarily at ∼260 nm in the UV region while those with high surface density (≥1.2 V/nm$^2$) exhibit a much broader absorption band in the UV region, and the absorption tail extends into visible region. This trend is consistent with the growth in domain size and change of coordination structure expected as more $VO_x$ is deposited on the surface.[11,31,32] Hydration of all samples leads to a slight broadening of the electronic absorption band, indicating some changes in coordination of the surface $VO_x$ species.

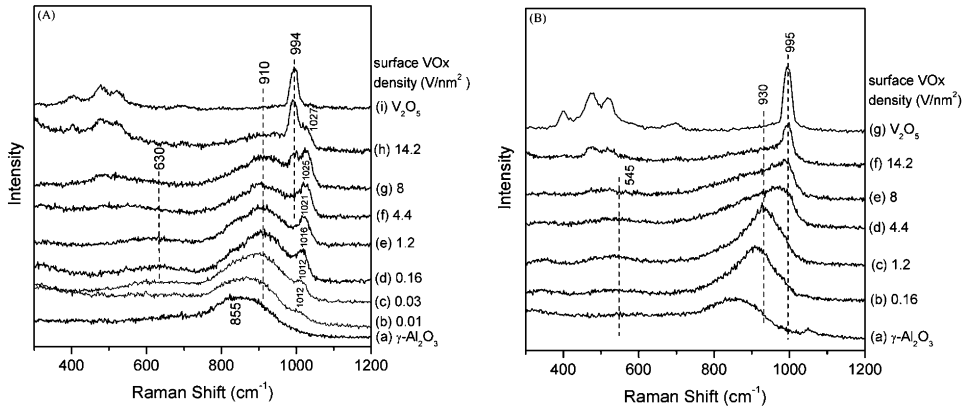


**Figure 4.** UV ($\lambda_{excitation}$ = 244 nm) Raman spectra of dehydrated (A) and hydrated (B) V/$\gamma$-$Al_2O_3$ as a function of surface $VO_x$ density (V/nm$^2$).

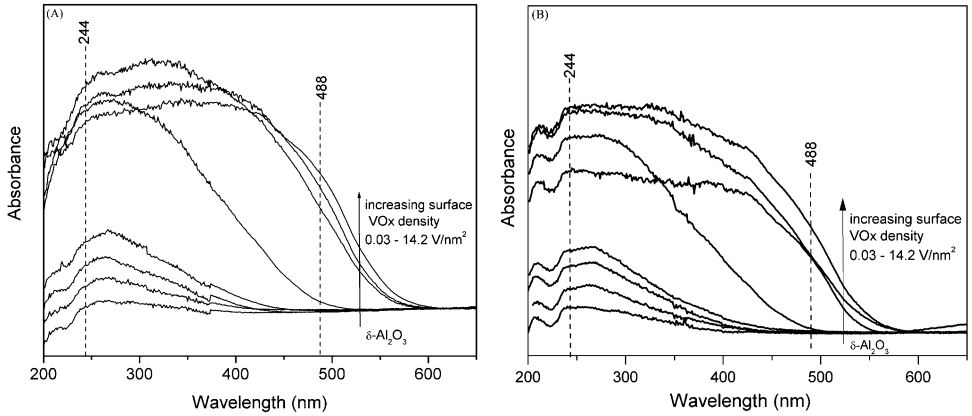


**Figure 5.** UV−vis DRS spectra of dehydrated (A) and hydrated (B) V/$\delta$-$Al_2O_3$ as a function of surface $VO_x$ density (V/nm$^2$).

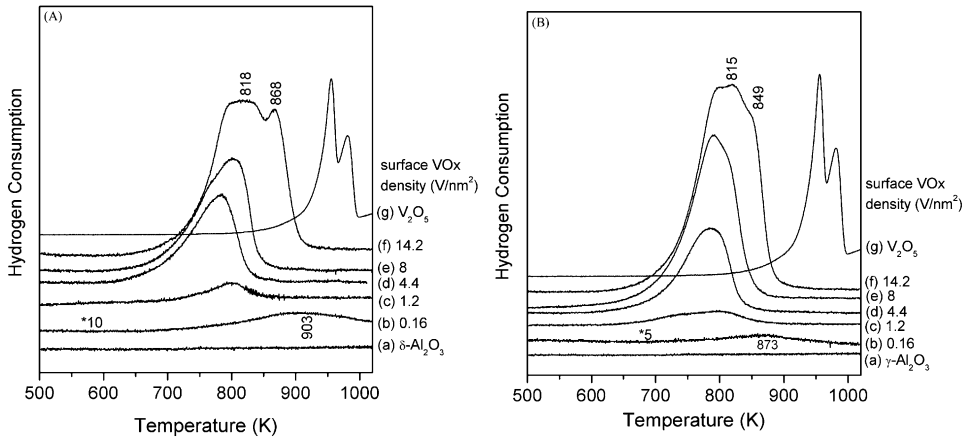


**Figure 6.** $H_2$ TPR profiles of (A) V/$\delta$-$Al_2O_3$ and (B) V/$\gamma$-$Al_2O_3$ as a function of surface $VO_x$ density (V/nm$^2$).

Supported vanadia catalysts have been extensively studied using UV−vis DRS, and the spectra were usually very broad.[11,31,32,33] By comparison with those of model vanadium compounds,[32] UV−vis absorption bands at around 240 and 290 nm were assigned to tetrahedrally coordinated monovanadate. The bands at 270, 340, and 412 nm have been ascribed to polyvanadate in either tetrahedral or pentahedral coordination.[31] Crystalline $V_2O_5$ shows several bands in the range 220−650 nm.[33] Thus, the UV−vis spectra in Figure 5A imply that tetrahedral $VO_x$ species are present on the support surface at surface densities below 1.2 V/nm$^2$ while pentahedral $VO_x$ and $V_2O_5$ are the main species at surface densities above 1.2 V/nm$^2$. When the dehydrated samples were hydrated, the UV−vis spectra were slightly broadened, suggesting that polyvanadate species exist to a larger extent on the support.

The UV−vis spectral features observed on dehydrated and hydrated V/$\gamma$-$Al_2O_3$ are similar to those on V/$\delta$-$Al_2O_3$ and not shown here, implying a similar coordination structure of $VO_x$ species on both $\gamma$-$Al_2O_3$ and $\delta$-$Al_2O_3$ in either the hydrated or dehydrated state. It should be noted that UV−vis spectra of V/$Al_2O_3$ samples with surface densities lower than 0.12 V/nm$^2$ have not been studied previously and those of V/$Al_2O_3$ with surface density higher than 0.12 V/nm$^2$ do not show significant difference from what have been reported for V/$Al_2O_3$ in the literature.[14,33]

**3.3. $H_2$ TPR Profiles.** Parts A and B of Figure 6 present the TPR profiles of $VO_x$ supported on $\delta$- and $\gamma$-$Al_2O_3$, respectively. The TPR profiles of the aluminas and $V_2O_5$ are also shown for comparison. The pure aluminas do not show evident reduction in the temperature range of room temperature through 1023 K. Reduction of $V_2O_5$ results in two sharp peaks at 956 and 981 K, similar to the profiles for $V_2O_5$ reported previously.[34] For all supported $VO_x$ samples, the reduction peak maxima shift as a function of surface $VO_x$ density, i.e., to lower temperatures and then back to higher temperatures, in agreement with data for V/$Al_2O_3$ found in the literature.[35,36] For example, in Figure 6A, the peak maximum at ∼903 K for 0.16 V shifts to 802 K for 1.2 V, to 784 K for 4.4 V, back to 803 K for 8 V, and to 818 K with a split at 868 K for 14.2 V. In the case of $\gamma$-$Al_2O_3$-supported $VO_x$ (Figure 6B), the maximum of the reduction peak is at ∼873 K for the 0.16-V sample; it shifts to 805 K for 1.2 V, to 787 K for 4.4 V, to 791 K for 8 V, and to 815 K with a shoulder at 849 K for 14.2 V.

## 4. Discussion

**4.1. Structures of Supported $VO_x$ Species.** Raman spectra of vanadia supported on aluminas (mainly $\gamma$-$Al_2O_3$) under hydrated and dehydrated conditions have been extensively researched.[3−14,17,18,27−29,35,37−40] These literature studies were usually based on the investigation of V/$\gamma$-$Al_2O_3$ with $VO_x$ loading in the range 1−30%, corresponding to surface densities of approximately 0.3−34.2 V/nm$^2$, depending on the surface area of the $\gamma$-$Al_2O_3$ used.[9,12] In our Raman studies, supported vanadia species were investigated on two different aluminas with surface $VO_x$ densities in the range 0.01−14.2 V/nm$^2$. $VO_x$ samples with higher surface density were not studied because $V_2O_5$ already formed when surface $VO_x$ density is above 8 V/nm$^2$ (see Figures 1−4). However, we did investigate V/$Al_2O_3$ samples with extremely low surface $VO_x$ density (down to 0.01 V/nm$^2$), which would give meaningful information on the initial structure of surface $VO_x$ species and their interactions with $Al_2O_3$. Depending on the surface $VO_x$ density, several sets of Raman bands are observed in the Raman spectra of V/$Al_2O_3$ samples: a broad one in the range 500−700 cm$^{-1}$, an intense one at 995 cm$^{-2}$, a broad one at ∼910 cm$^{-1}$, and sharp bands in the range 1010−1035 cm$^{-1}$. The former two bands are obviously due to V−O−V vibration and $V_2O_5$, respectively. We focus our attention on the latter two sets of Raman bands as they provide more structural information on the supported $VO_x$ species.

The assignment of the bands above 1000 cm$^{-1}$ is straightforward: it is due to the V═O stretching vibration. It is interesting that two kinds of shift of this band can be distinguished: a shift as a function of excitation wavelength for the same sample and a shift as a function of surface $VO_x$ density for different samples. The former shift is caused by different $VO_x$ structures detected at different excitations and will be further discussed in section 4.2. The latter shift, from 1012 to 1027 cm$^{-1}$ as the surface $VO_x$ density increases from 0.01 to 14.2 V/nm$^2$ in the case of UV-excited Raman spectra (see Figures 2 and 4), is due to changes in the $VO_x$ structure. With increasing surface coverage, $VO_x$ species evolve from monovanadates to polyvanadates and crystalline $V_2O_5$ on the $Al_2O_3$ support with evolving surface structures. A change in the surface structure would result in a change of the V═O bond length and/or its coupling to other bonds in the structure and thus the shift of V═O Raman band.[9,10,15,37] For example, Hardcastle and Wachs[35] surmised that the length of terminal V═O bonds in a large number of vanadium-containing model compounds changes with the structure and coordination of these compounds. They developed an empirical formula for relating the V−O band frequency to its bond length.

The broad Raman band at ∼910 cm$^{-1}$, conventionally attributed to V−O−V of polyvanadates, is observed on V/$Al_2O_3$

samples at all surface densities, even as low as 0.01 V/nm$^2$. Since it is unlikely that polymerized $VO_x$ has formed at these low loadings, this band should no longer be considered as an identification of polymerized $VO_x$. This point was also previously suggested by Deo et al.[3] but was not proved conclusively. Very recently, DFT calculations on the interaction of $VO_x$ with $Al_2O_3$ (both corundum and spinel structures)[27] concluded that the interface mode, V−O−Al, gives intense Raman band in the range 900−950 cm$^{-1}$ for $VO_x$ supported on $Al_2O_3$ with the spinel structure. Since both $\delta$- and $\gamma$-$Al_2O_3$ have the spinel-type structure and the broad Raman band at ∼910 cm$^{-1}$ is observed on V/$\delta$- and $\gamma$-$Al_2O_3$ even at the lowest coverages, this band is assigned to the V−O−Al interface mode. This band was observed in previous studies but was incorrectly assigned to the bridging V−O−V mode.[5−7,9,10,40] Previous Raman studies[5,6,10] assumed that the Raman cross section of interface V−O−Al vibrations is very small or zero. The direct observation of the interface mode in Raman spectroscopy is of significance to the understanding of redox reactions catalyzed by supported vanadia catalysts because the bridging V−O−S bond has been considered as a key active site for these reactions.[4−6,13,18]

A brief summary of the Raman results of vanadia supported on both $\delta$- and $\gamma$-$Al_2O_3$ can be made based on above assignments: Raman features due to V═O and V−O−Al vibrations are observed at surface densities as low as 0.01 V/nm$^2$; broad bands due to V−O−V vibrations and an intense band due to $V_2O_5$ appear at medium and high surface $VO_x$ density. By combination of the Raman results with the corresponding UV−vis DRS spectra (Figures 5), the structural evolution of surface $VO_x$ species on both aluminas can be described as follows: V/$Al_2O_3$ with a surface density lower than 1.2 V/nm$^2$ possesses mainly isolated $VO_x$ in tetrahedral coordination.[32,41] At surface densities higher than 1.2 V/nm$^2$, polymerized $VO_x$ participate to a larger extent on the surface, and $V_2O_5$ forms at a surface $VO_x$ density above 4.4 V/nm$^2$. Following this evolution picture of surface $VO_x$ species, it appears that the V═O stretches in isolated $VO_x$ species occur at lower wavenumbers than in polymerized $VO_x$ species (Figures 2 and 4). This observation is consistent with most literature results that the frequency of V═O stretches shows approximately a 10−15-cm$^{-1}$ shift to higher wavenumbers with increasing $VO_x$ coverage.[9,10] However, the opposite conclusion was also reported: isolated $VO_x$ species give rise to V═O stretches at higher wavenumbers than polymerized $VO_x$.[13] On the basis of this assignment and the reactivity tests, the authors concluded that isolated $VO_x$ species on $\gamma$-$Al_2O_3$ are more relevant to the oxidative dehydrogenation of propane.[13] But our results suggest that the assignment of the V═O stretching bands in ref 13 should be revised and that the conclusion based on this assignment should also be revised.

The TPR results of V/$\delta$- and $\gamma$-$Al_2O_3$ (Figure 6) provide further information on the distribution and reducibility of surface $VO_x$ species. The high-temperature peak at ca. 873−903 K is mainly due to isolated adsorbed vanadia species that bind strongly to the alumina support, presumably via three V−O−Al bonds. The reduction temperature of isolated $VO_x$ species is higher than normal oxidative dehydrogenation and even dehydrogenation reaction temperatures. This indicates that isolated $VO_x$ species may not play a critical role in these reactions. The reduction peak at 783−823 K can be attributed to clustered $VO_x$ species. And the peak/shoulder at around 843−873 K is assigned to well-dispersed $V_2O_5$, which possesses a very small particle size and thus is easier to reduce than unsupported bulk $V_2O_5$. It is expected that this peak would approach those of bulk $V_2O_5$ when the surface $VO_x$ density increases further. By considertion of the areas of the reduction peaks due to $V_2O_5$ and polyvanadates, $V_2O_5$ has not become the main surface species at surface densities up to 14.2 V/nm$^2$, even though the $V_2O_5$ bands dominate the Raman spectra (e.g., Figures 1−4). Their strong intensity is due to the much larger Raman cross section of $V_2O_5$ compared to dispersed vanadia species.[26] The similarity of the TPR profiles of vanadia on $\delta$- and $\gamma$-$Al_2O_3$ shows that the support phase (environment) has little effect on the reducibility of the three surface VOx species.

For hydrated V/$Al_2O_3$ samples, the surface vanadia species were found to depend on the net pH at the point of zero charge of the surface and can be predicted from the known vanadia aqueous phase diagram.[3−6,8,39] In reference to the previous Raman study of vanadia on $\gamma$-$Al_2O_3$,[8] the broad band from 920 to 990 cm$^{-1}$ on V/$\delta$- and $\gamma$-$Al_2O_3$ (Figures 2B and 4B) can be assigned to V═O stretching in the polyvanadate structure. The hydrolysis of the terminal V═O bond and interface V−O−Al bonds under ambient conditions by water moisture leads to the aggregation of surface $VO_x$ into polyvanadates.[8,39] This conclusion is supported by the UV−vis DRS spectra of hydrated V/$\delta$- and $\gamma$-$Al_2O_3$ (see Figure 6B), which show broadened absorption bands compared to the corresponding dehydrated samples (Figure 6A). The Raman study of supported $VO_x$ in the hydrated state is potentially useful for providing structural information on surface $VO_x$ in reactions where moisture is present in the feed gas or as a reaction product. Thus the properties of supported $VO_x$ under reaction conditions can be better understood.

The Raman, UV−vis DRS and $H_2$ TPR results indicate that the structure, distribution, and reducibility of surface $VO_x$ species on $\delta$- and $\gamma$-$Al_2O_3$ are quite similar. This similarity is understandable since both $\delta$- and $\gamma$-$Al_2O_3$ have a spinel structure with similar types (but different distribution) of surface hydroxyl groups,[41,43] which are the bonding sites for $VO_x$ species on the aluminas. Some slight spectral differences between V/$\gamma$-$Al_2O_3$ and V/$\delta$-$Al_2O_3$ are discernible. In the visible Raman spectra (Figures 1 and 3), bands due to surface $VO_x$ species can be detected on V/$\delta$-$Al_2O_3$ at a surface density of 0.16 V/nm$^2$ while $VO_x$ species on $\gamma$-$Al_2O_3$ are only detectable at 1.2 V/nm$^2$, suggesting that $VO_x$ species feature a higher dispersion on the surface of $\gamma$-$Al_2O_3$ than on $\delta$-$Al_2O_3$. The higher dispersion of $VO_x$ on $\gamma$-$Al_2O_3$ is evidenced by the spectra at higher surface density: the band at ca. 1035 cm$^{-1}$, due to dispersed $VO_x$, is still observable at a surface density of 8 V/ nm$^2$ on $\gamma$-$Al_2O_3$ (Figure 3) while it has disappeared on V/$\delta$-$Al_2O_3$ (Figure 1); the intensity ratio of the bands at 995 and 1026 cm$^{-1}$ is smaller for V/$\gamma$-$Al_2O_3$ at the surface density of 8 V/nm$^2$ (Figure 4) than for V/$\delta$-$Al_2O_3$ (Figure 2). The $H_2$ TPR profiles also show that $VO_x$ species are better dispersed on $\gamma$-$Al_2O_3$ than on $\delta$-$Al_2O_3$ because the reduction peak due to $V_2O_5$ at around 849−873 K is more evident for V/ $\delta$-$Al_2O_3$ than V/$\gamma$-$Al_2O_3$ at the same surface density of 14.2 V/nm$^2$ (Figure 6). This is consistent with our motivation for comparing vanadia on $\delta$- and $\gamma$-$Al_2O_3$ because the density of surface hydroxyl groups on the two aluminas was thought to be different.[43] More reactive hydroxyl groups were found on $\gamma$-$Al_2O_3$ than on $\delta$-$Al_2O_3$ so that $\delta$-$Al_2O_3$ is less active than $\gamma$-$Al_2O_3$.[44] This explains the better dispersion of $VO_x$ species on $\gamma$-$Al_2O_3$ than on $\delta$-$Al_2O_3$.

**4.2. Multiline Excitation: UV vs Visible Excitation.** The initial motivation for using different excitation laser lines was to investigate the use of the resonance enhancement effect to selectively detect different structures of vanadia on $Al_2O_3$. This possibility has been shown by the Raman and UV−vis DRS

results presented here. To use dehydrated V/$\delta$-$Al_2O_3$ as an example, a comparison of the Raman spectra excited by visible laser (Figure 1A) to those excited by UV laser (Figure 2A) shows at least three differences between the UV and visible spectra:

(1) UV Raman spectra show clear Raman bands due to supported $VO_x$ species at surface densities much lower than in visible Raman spectra. On one hand, this is due to the low signal levels and interference from fluorescence on $Al_2O_3$ in visible Raman when the surface $VO_x$ density is very low (e.g., $<0.16$ V/nm$^2$). On the other hand, the avoidance of fluorescence and the resonance enhancement of isolated $VO_x$ species in UV Raman make them detectable. The selective resonance enhancement effect is evidenced by the UV−vis DRS spectra of V/$\delta$-$Al_2O_3$ (Figure 5A). When the surface density is lower than 1.2 V/nm$^2$, the electronic absorption band occurs only in the UV region where 244-nm excitation leads to the resonance Raman effect while 488-nm excitation is not resonance enhanced.

(2) The spectra of the same sample show V═O stretching bands at different Raman shifts, 8−10 cm$^{-1}$ lower in UV Raman than in visible Raman, indicating that UV and visible excitations detect different $VO_x$ species present on the support. This kind of band shift can also be explained in terms of the resonance enhancement effect. The UV−vis absorption spectra of V/$\delta$-$Al_2O_3$ (Figure 5A) show significant absorption bands at both 244- and 488-nm laser wavelengths for samples with surface densities above 1.2 V/nm$^2$, which implies that the Raman spectra at both wavelengths are resonance enhanced. The longer wavelength absorption increases in intensity with vanadia loading, relative to the short wavelength absorption. This demonstrates that a mixture of surface vanadia species is present and is consistent with a picture where polymerized $VO_x$ species are resonance enhanced under visible laser excitation, while isolated and less polymerized $VO_x$ are resonance enhanced under UV laser excitation. The selective enhancement of $VO_x$ species with different cluster sizes is similar to the case of resonance Raman spectroscopic characterization of conjugated polyene sequences where different excitation wavelengths give different C═C stretching frequencies, and thus conjugated polyenes with different sequence lengths are detected.[45] Interestingly, the higher V═O Raman shift measured under visible compared to UV excitation is consistent with this picture by reference to the measurements on the model catalysts since the V═O infrared frequencies are found to increase with increasing V═O surface density.[46] Thus, it would appear that visible-excited Raman spectra are more sensitive to polymeric or cluster $VO_x$ and that UV-excited Raman spectra are more sensitive to isolated and less polymerized $VO_x$ species.

(3) The V═O stretching band at 995 cm$^{-1}$ characteristic of $V_2O_5$ is seen at lower surface $VO_x$ densities in visible Raman spectra (Figure 1) than in UV Raman spectra (Figure 2). For example, this band is detected at a surface density of 4.4 V/nm$^2$ under visible excitation, while it is only observable at surface densities above 8 V/nm$^2$ under UV excitation. This is due to the different absorption properties of $V_2O_5$ in both UV and visible regions. Though $V_2O_5$ shows electronic absorption in both regions,[33] the absorption is much stronger in the UV region, and fewer scatterers contribute to the spectrum in UV Raman compared to visible Raman. Thus, UV Raman is less sensitive for monitoring crystalline $V_2O_5$ than visible Raman. This is more obvious in the measurement of unsupported $V_2O_5$, which shows that a comparable UV Raman spectrum requires a collection time typically three times longer than with visible wavelength excitation under similar experimental conditions. It is also in agreement with the principle that the Raman cross section is frequency dependent. Actually the influence of absorption on Raman spectra is also quite evident when the surface $VO_x$ density is very low for either V/$\delta$-$Al_2O_3$ (Figure 2) or V/$\gamma$-$Al_2O_3$ (Figure 4). For example, the strong Raman bands due to $\delta$-$Al_2O_3$ are hardly detectable even at a surface density of 0.16 V/nm$^2$ (Figure 2), which is too small to completely cover the support surface. This is obviously due to the strong absorption of UV radiation by surface $VO_x$ species.

## 5. Conclusions

The surface vanadia species supported on $\delta$- and $\gamma$-$Al_2O_3$ with surface density of 0.01−14.2 V/nm$^2$ have been characterized under both hydrated and dehydrated conditions using both UV and visible Raman spectroscopy and UV−vis DRS. TPR was also employed to provide additional information on the structure and reducibility of the surface $VO_x$ species.

(1) Three kinds of surface $VO_x$ species are dispersed on the two aluminas under dehydrated conditions: isolated $VO_x$ species are present at surface density below 1.2 V/nm$^2$; polyvanadates starts to be the main surface species at surface densities in the range 1.2−14.2 V/nm$^2$; $V_2O_5$ readily forms on the surface at a surface density higher than 4.4 V/nm$^2$. The structure, distribution, and reducibility of dehydrated surface $VO_x$ species are similar on both $\delta$- and $\gamma$-$Al_2O_3$ with the exception that $VO_x$ species are little better dispersed on $\gamma$-$Al_2O_3$ than on $\delta$-$Al_2O_3$ due to differences in the density of surface hydroxyl groups. The surface $VO_x$ species behave similarly upon hydration on both aluminas, and polyvanadates are the main surface species. In summary, there exist only minor differences in dispersed $VO_x$ species on the two aluminas.

(2) The broad Raman band at ca. 910 cm$^{-1}$, previously assigned to V−O−V vibrations in polyvanadates, is observed on V/$Al_2O_3$ with surface densities as low as 0.01 V/nm$^2$ and is assigned to the interface mode (V−O−Al). This bridging bond has been considered as the key active site for the redox reactions catalyzed by supported $VO_x$. The reassignment of this band makes it possible to get further insights into the redox mechanism via in situ Raman spectroscopy.

(3) Because of the resonance enhancement effect and the avoidance of fluorescence in UV Raman spectroscopy, UV Raman can provide structural information on $VO_x$ species at extremely low surface $VO_x$ density (down to 0.01 V/nm$^2$), where the $VO_x$ is not detectable by visible Raman. At higher surface $VO_x$ density, UV Raman shows higher sensitivity to isolated and less polymerized $VO_x$ species while visible Raman is more sensitive to highly polymerized $VO_x$ species and crystalline $V_2O_5$, which is explained in terms of a selective resonance enhancement effect as evidenced by UV−vis DRS results. The present study suggests that a complete structural characterization of supported metal oxide catalysts requires a multiwavelength excitation approach in Raman spectroscopy.

**Acknowledgment.** This work is financially supported by ATHENA and the Chemical Sciences, Geosciences and Biosciences Division, Office of Basic Energy Sciences, Office of Science, U.S. Department of Energy under Grant No. DE-FG02-97ER14789. The ATHENA project is funded by the Engineering & Physical Sciences Research Council (EPSRC) of the U.K. and Johnson Matthey plc. We acknowledge Dr. Meijun Li for assistance in TPR measurements.

## References and Notes

(1) Bond, G. C.; Tahir, S. F. *Appl. Catal.* **1991**, *71*, 1.

(2) Reddy, B. N.; Reddy, B. M.; Subrahmanyam, M. *J. Chem. Soc., Faraday Trans*. **1991**, *87*, 1649.
(3) Deo, G.; Wachs, I. E.; Haber, J. *Crit. Rev. Surf. Chem*. **1994**, *4*, 141.
(4) Wachs, I. E.; Weckhuysen, B. M. *Appl. Catal., A* **1997**, *157*, 67.
(5) Bañares, M. A.; Wachs, I. E. *J. Raman Spectrosc*. **2002**, *33*, 359.
(6) Weckhuysen, B. M.; Keller, D. E. *Catal. Today* **2003**, *78*, 25.
(7) Went, G. T.; Oyama, S. T.; Bell, A. T. *J. Phys. Chem.* **1990**, *94*, 4240.
(8) Deo, G.; Wachs, I. E. *J. Phys. Chem.* **1991**, *95*, 5889.
(9) Vuurman, M. A.; Wachs, I. E. *J. Phys. Chem.* **1992**, *96*, 5008.
(10) Wachs, I. E. *Catal. Today* **1996**, *27*, 437.
(11) Olthof, B.; Khodakov, A.; Bell, A. T.; Iglesia, E. *J. Phys. Chem. B* **2000**, *104*, 1516.
(12) Argyle, M. D.; Chen, K. D.; Bell, A. T.; Iglesia, E. *J. Catal*. **2002**, *208*, 139.
(13) Cortez, G. G.; Bañares, M. A. *J. Catal*. **2002**, *209*, 197.
(14) Khodakov, A.; Olthof, B.; Bell, A. T.; Iglesia, E. *J. Catal*. **1999**, *181*, 205.
(15) Christodoulakis, A.; Machli, M.; Lemonidou, A. A.; Boghosian, S. *J. Catal*. **2004**, *222*, 293.
(16) Xiong, G.; Li, C.; Li, H. Y.; Xin, Q.; Feng, Z. C. *Chem. Commun.* **2000**, 677.
(17) Chua, Y. T.; Stair, P. C.; Wachs, I. E. *J. Phys. Chem. B* **2001**, *105*, 8600.
(18) Wachs, I. E.; Jehng, J. M.; Deo, G.; Weckhuysen, B. M.; Guliants, V. V.; Benziger, J. B.; Sundaresan, S. *J. Catal.* **1997**, *170*, 75.
(19) Xiong, G.; Li, C.; Feng, Z. C.; Ying, P. L.; Xin Q.; Liu, J. K. *J. Catal* **1999**, *186*, 234.
(20) Xiong, G.; Feng, Z. C.; Li, J.; Yang, Q. H.; Ying, P. L.; Xin Q.; Li, C. *J. Phys. Chem. B* **2000**, *104*, 3581.
(21) Li, C.; Stair, P. C. *Stud. Surf. Sci. Catal.* **1996**, *101*, 881.
(22) Stair, P. C.; Li, C. *J. Vac. Sci. Technol. A* **1997**, *15*, 1679.
(23) Lippens, B. C.; Steggerda, J. J. In *Physical and Chemical Aspects of Adsorbents and Catalysts*; Linsen, B. C., Ed.; Academic Press: New York, 1970; p 171.
(24) Wilson, S. J.; McConnell, J. D. C. *J. Solid State Chem.* **1980**, *34*, 315.
(25) Chua, Y. T.; Stair, P. C. *J. Catal.* **2000**, *196*, 66.
(26) Xie, S. B.; Iglesia, E.; Bell, A. T. *Langmuir* **2000**, *16*, 7162.
(27) Magg, N.; Immaraporn, B.; Giorgi, J. B.; Schroeder, T.; Bäumer, M.; Döbler, J.; Wu, Z. L.; Kondratenko, E.; Cherian, M.; Baerns, M.; Stair, P. C.; Sauer, J.; Freund, H. J. *J. Catal.* **2004**, *226*, 88.
(28) Deo. G.; Hardcastle, F. D.; Hirt, A. M.; Wachs, I. E. *ACS Symp. Ser*. **1990**, *437*, 317.
(29) Hardcastle, F. D.; Richards, M.; Deo, G.; Wachs, I. E. *Abstr. Pap. Am. Chem. Soc.* **1989**, *198*, 34.
(30) Lever, A. B. P. *Inorganic Electronic Spectroscopy*; Elsevier: New York, 1968.
(31) Arena, F.; Frusteri, F.; Martra, G.; Coluccia, S.; Parmaliana, A. *J. Chem. Soc., Faraday Trans*. **1997**, *93*, 3849.
(32) Schraml-Marth, M.; Wokaun, A.; Pohl, M.; Krauss, H. L. *J. Chem. Soc., Faraday Trans.* **1991**, *87*, 2635 and references therein.
(33) Gao, X. T.; Wachs, I. E. *J. Phys. Chem. B* **2000**, *104*, 1261.
(34) Koranne, M. M.; Goodwin, J. G., Jr.; Marcelin, G. *J. Catal.* **1994**, *148*, 369.
(35) Kanervo, J. M.; Harlin, M. E.; Krause, A. O.; Bañares, M. A. *Catal. Today* **2003**, *78*, 171.
(36) Stobbe-Kreemers, A. W.; van Leerdam, G. C.; Jacobs, J. P., Brongersma, H. H.; Scholten, J. J. F. *J. Catal.* **1995**, *152*, 130.
(37) Hardcastle, F. D.; Wachs, I. E. *J. Phys. Chem.* **1991**, *95*, 5031.
(38) Coustumer, L. R. L.; Taouk, B.; Meur, M. L.; Payen, E.; Guelton, M.; Grimblot, J. *J. Phys. Chem.* **1988**, *92*, 1231.
(39) Jehng, J. M.; Deo, G.; Weckhuysen, B. M.; Wachs, I. E. *J. Mol. Catal., A* **1996**, *110*, 41.
(40) Bañares, M. A.; Martínez-Huerta, M. V.; Gao, X.; Fierro, J. L. G.; Wachs, I. E. *Catal. Today* **2000**, *61*, 295.
(41) Ruitenbeek, M.; van Dillen, A. J.; de Groot, F. M. F.; Wachs, I. E.; Geus, J. W.; Koningsberger, D. C. *Top. Catal.* **2000**, *10*, 241.
(42) Knözinger, H.; Ratnasamy, P. *Catal. Rev. Sci. Eng*. **1978**, *17*, 31.
(43) Tsyganenko, A. A.; Mardilovich, P. P. *J. Chem. Soc., Faraday Trans.* **1996**, *92*, 4843.
(44) Morterra, C.; Magnacca, G. *Catal. Today* **1996**, *27*, 497.
(45) Gerrard, D. L.; Maddams, W. F. *Macromolecules* **1981**, *14*, 1356.
(46) Magg, N.; Giorgi, J. B.; Schroeder, T.; Bäumer, M.; Freund, H. J. *J. Phys. Chem. B* **2002**, *106*, 8756.